PCCP

ROYAL SOCIETY OF CHEMISTRY

PAPER

View Article Online
View Journal | View Issue

Check for updates

Cite this: *Phys. Chem. Chem. Phys.*, 2022, **24**, 8113

Bimolecular reactions of S^{2+} with Ar, H_2 and N_2: reactivity and dynamics†

Sam Armenta Butt* and Stephen D. Price *

Received 25th November 2021,
Accepted 17th March 2022

DOI: 10.1039/d1cp05397c

rsc.li/pccp

The reactivity, energetics and dynamics of bimolecular reactions between S^{2+} and three neutral species (Ar, H_2 and N_2) have been studied using a position-sensitive coincidence methodology at centre-of-mass collision energies below 6 eV. This is the first study of bimolecular reactions involving S^{2+}, a species detected in planetary ionospheres, the interstellar medium, and in anthropogenic manufacturing processes. The reactant dication beam employed consists predominantly of S^{2+} in the ground ^3P state, but some excited states are also present. Most of the observed reactions involve the ground state of S^{2+}, but the dissociative electron transfer reactions appear to exclusively involve excited states of this atomic dication. We observe exclusively single electron-transfer between S^{2+} and Ar, a process which exhibits strong forward scatting typical of the Landau–Zener style dynamics observed for other dicationic electron transfer reactions. Following collisions between S^{2+} + H_2, non-dissociative and dissociative single electron-transfer reactions were detected. The dynamics here show evidence for the formation of a long-lived collision complex, $[SH_2]^{2+}$, in the dissociative single electron-transfer channel. The formation of SH^+ was not observed. In contrast, the collisions of S^{2+} + N_2 result in the formation of SN^+ + N^+ in addition to the products of single electron-transfer reactions.

Open Access Article. Published on 22 March 2022. Downloaded on 2/21/2026 4:14:56 PM.
This article is licensed under a Creative Commons Attribution 3.0 Unported Licence.

Introduction

Doubly charged positive ions (dications) can be found in energised environments such as the ionospheres of planets and their satellites,[1–8] the interstellar medium,[9–11] and in anthropogenic plasmas.[12–14] Significant bimolecular reactivity is shown following collisions of both atomic and molecular dications with neutral species in the gas-phase.[15–20] The lifetimes of atomic dications in planetary ionospheres are expected to be primarily determined by such collisional processes.[21] In addition, despite their usual inherent thermodynamic instability, the metastable electronic states of molecular dications have been shown to possess lifetimes sufficient to allow collisions with other species in ionospheres and elsewhere.[15] Given the above lifetimes, the demonstrated bimolecular reactivity of these dications strongly suggests that dication chemistry can play a role in ionospheric processes;[22] for example, dications could be involved in the chemistry of complex molecule formation through reactions involving carbon chain-growth.[21,23–26]

There are numerous examples of the detection of atomic dications in planetary ionospheres.[27] However, it is difficult to unambiguously detect molecular dications in ionospheres using simple mass spectrometry, the usual sampling technique. This difficulty arises because these environments often contain monocations with the same mass to charge ratio as the target dication.[15] The historical absence of a definitive detection of ionospheric molecular dications may account for the relative neglect of these species in models of ionosphere chemistry.[21] Encouragingly, the presence of the CO_2^{2+} dication in the ionosphere of Mars has been recently confirmed, the first detection of a molecular dication in such an environment.[28] In order to identify dication reactions of ionospheric interest, laboratory-based experiments to probe dicationic reactivity, along with further *in situ* detection of dications in ionospheres, are vital.[29] Indeed, recognition of the presence of molecular dications in planetary atmospheres has led to the identification of the role these species can play in atmospheric erosion.[30–33] To develop further our understanding of dicationic processes, this paper presents an investigation of the reactions of S^{2+} with Ar, H_2 and N_2. This work reveals the reactivity, reaction mechanisms and reaction energetics of S^{2+}, extending and enhancing our understanding of the chemistry of dications in environments such as planetary atmospheres.

Sulfur-containing species are found in a wide variety of astrophysical environments[34–37] and on Earth, where they are ubiquitous both in nature and from anthropogenic activities.[38,39] The S^{2+} ion has been observed in both terrestrial and non-terrestrial environments. For example, when plasmas

Department of Chemistry, University College London, 20 Gordon Street, London, WC1H 0AJ, UK. E-mail: sam.butt.16@ucl.ac.uk, s.d.price@ucl.ac.uk; Fax: +44 (0)20 7679 7463; Tel: +44 (0)20 7679 4600, +44 (0)20 7679 4606

† Electronic supplementary information (ESI) available. See DOI: 10.1039/d1cp05397c

Open Access Article. Published on 22 March 2022. Downloaded on 2/21/2026 4:14:56 PM.
This article is licensed under a Creative Commons Attribution 3.0 Unported Licence.

involving SF_6 are used for etching, S^{2+} can be formed.[40,41] In interstellar clouds, organic compounds containing sulfur have been detected, including species with S–X bonds where X = O, C, N, H,[34] and S^{2+} has been observed in nebulae close to sources of high energy photons.[42–44] Indeed, the reactions of the sulfur dication are thought to be important in the ionosphere of Io, the satellite of Jupiter, where S^{2+} has been detected by the Galileo[27] and Voyager I[45,46] spacecraft, as well as by the Hubble telescope.[47] Io's sulfur-rich atmosphere is derived from this moon's intense volcanic activity which results in the expulsion of SO_2.[48,49] Hence, S^{2+} is thought to be one of the major species in the Io torus,[50] a region of the Jovian system where charged species generated in Io's ionosphere, such as S^{2+}, are transferred to Jupiter, dominating both the planets magnetosphere[49,51] and the torus of Europa.[52] Despite this clear relevance of S^{2+} to astrophysical and anthropogenic environments, and the longevity of the atomic dication, there are no reports in the literature (to the authors' knowledge) of the bimolecular reactivity of S^{2+} dications in the gas phase. Therefore, the investigation of the collisions of S^{2+} with neutral molecules presented in this study provides the first experimental information on the reactivity of this ion; that information is particularly pertinent to the chemistry of a number of astrophysical and terrestrial environments.

As a first investigation of the chemistry of S^{2+}, we have chosen to study the reactions with three neutral gases that are important in interstellar and atmospheric chemistry: Ar, H_2 and N_2. Argon is often present in significant concentrations in planetary atmospheres.[53–55] H_2 is the most abundant molecule in the universe and is the dominant species making up the gaseous planets, including Jupiter.[56–58] Molecular nitrogen (N_2) is important in the atmospheres of terrestrial bodies in the solar system, especially the Earth and Titan where it is the dominant species.[21,22,54,55,59–63]

The reactions resulting from dication collisions with argon have been well studied. Single electron-transfer (SET) was observed in collisions with rare gas dications: Ne^{2+}, Ar^{2+}, Kr^{2+} or Xe^{2+}.[64–69] Collisions between N_2^{2+} and Ar also resulted in the observation of SET reactions.[70] Collisions between Ar and hydrogen-containing dications, such as CHX^{2+} (X = F, Cl, Br, I), often result in SET and proton-transfer (PT) reactions; the latter, for example, forming ArH^+.[71–73] Interactions between Ar and SF_x^{2+} (x = 2–4) or CF_y^{2+} (y = 1–3) have been the subject of several studies, with SET and collision-induced dissociation (CID) channels being observed.[74–78] Additionally, some dication reactions with Ar have been shown to generate product dications involving new chemical bonds. For example, $HCCAr^{2+}$ and $ArCF_2^{2+}$ are detected following collisions of Ar with $C_2H_2^{2+}$ and CF_3^{2+} respectively.[79,80]

A variety of dication reactions with H_2 have been studied at low collision energies, often resulting in SET reactions. Reactions between Ar^{2+} and H_2 resulted in non-dissociative and dissociative SET (NDSET and DSET respectively).[64,66,81] With some H-containing dications (for example $CHCl^{2+}$) H^+ transfer to the neutral H_2 is observed, producing H_3^+ *via* the formation of collision complexes.[82–84] Direct hydride (H^-) transfer from the H_2 to the dication is also seen in some systems.[83,85] Many other bond-forming channels have been observed in dication reactions with H_2, often with evidence that the reactions proceed *via* complexation.[17,86–89] Some of the new bonds formed in this class of reaction include N–H,[89] H–H,[84] C–H,[82,83,85–88] F–H,[17,87,88] Cl–H,[83] and Br–H.[82] The ubiquity of bond-forming reactions in dication/H_2 collision systems, and the prevalence of S–H bonds in nature, marks out the S^{2+} + H_2 collision system as a candidate for the generation of new bonds.

The reactions following dication collisions with N_2 have been the subject of several previous studies, including recent work by the current authors.[90] In the Ar^{2+} + N_2 collision system, SET, double electron-transfer (DET) and bond-forming pathways were observed.[64,66–68,81,90–92] SET channels were also reported following the interactions of N_2 with CO^{2+} and N_2^{2+}.[93,94] DSET resulting from the collisions of Ne^{2+} + N_2 was shown to occur *via* two mechanisms, one involving a collision complex.[95] Bond-forming reactions have been observed following the interactions of N_2 with $C_4H_3^{2+}$ and O_2^{2+}, resulting in the formation of N–H and N–O bonds.[84,96] Additionally, S–N bond-formation has been observed following the gas-phase collisions of S^+ ions with ammonia.[97]

In our experiments, we collide S^{2+} ions with the selected neutral species using a Position-Sensitive Coincidence Mass Spectrometer (PSCO-MS), at centre-of-mass (CM) collision energies of less than 6 eV. The PSCO-MS combines coincident detection of product cations with a crossed-beam methodology. The results from our experiments give a detailed insight into the reactivity and dynamics of dication–neutral interactions. For example, SET reactions are observed following the interactions of S^{2+} with Ar, N_2 and H_2, including both non-dissociative and dissociative channels with the molecular targets. The collisions of S^{2+} with N_2 also result in the formation of SN^+ + N^+ *via* a collision complex. The dynamics of the DSET channel in the S^{2+} + H_2 system also shows evidence for the formation of a collision complex, $[SH_2]^{2+}$.

Experimental

Coincidence techniques involve the simultaneous detection of two or more products from a single reactive event. Dication interactions with neutrals often generate pairs of monocations, and these pairs of ions are detected in coincidence in our PSCO-MS experiment, which has been described in detail in the literature.[76,98,99] In brief, a pulsed beam of dications is directed into the field-free source region of a time-of-flight mass spectrometer (TOF-MS). In this region the dications interact with a jet of the neutral reactant. Subsequent application of an extraction voltage to the source region allows the TOF-MS to detect the cation pairs generated from the dication-neutral interactions. The detection of these ions involves recording their arrival time, and position, at a large microchannel-plate detector. From this raw data, a list of flight times and arrival positions of the ions detected in pairs, a two-dimensional mass spectrum, can be generated revealing the different reactive

 This journal is © the Owner Societies 2022

Open Access Article. Published on 22 March 2022. Downloaded on 2/21/2026 4:14:56 PM.
This article is licensed under a Creative Commons Attribution 3.0 Unported Licence.

channels. The positional data accompanying the ionic detections yields the relative motion of the products of each reactive event, providing a detailed insight into the mechanisms of each reactive channel.[99]

The S^{2+} ions used in the experiments described in this paper were generated *via* electron ionization of H_2S (CKgas, 99.5%) by 100 eV electrons in a custom-built ion source. Previous investigations show that S^{2+} (m/z = 16), HS^{2+} (m/z = 16.5), and H_2S^{2+} (m/z = 17) dications are all formed following the bombardment of H_2S with electrons.[100] The positively charged ions are extracted from the ion source and pass through a hemispherical energy analyser to restrict the translational energy spread of the final S^{2+} beam to $\sim$0.3 eV. The continuous beam of ions exiting the hemispherical analyser is then pulsed, using a set of electrostatic deflectors, before being accelerated and focussed into a commercial velocity filter. The velocity filter is set to transmit just the $^{32}S^{2+}$ (m/z = 16) ions. O^+ ions, generated from the ionization of background gases in the ion source, may also be present in our dication beam because O^+ has the same m/z ratio as $^{32}S^{2+}$. However, reactions involving O^+ ions will not result in the generation of two cationic products. Therefore, the products of reactions involving these contaminant O^+ ions will not contribute to our coincidence spectra. The resulting pulsed beam of energy-constrained S^{2+} ions is then decelerated to $<$10 eV in the laboratory frame before entering the source region of the TOF-MS. In the TOF-MS source region the beam of dications is crossed with an effusive jet of the appropriate neutral species: Ar (BOC, 99.998%), H_2 (BOC, $>$99.995%), or N_2 (BOC, $>$99.998%). Single-collision conditions[101] are achieved by employing an appropriately low pressure of the neutral collision partner. Under these conditions most dications do not undergo a collision and only a small percentage experience one collision. Such a pressure regime ensures no secondary reactions, due to successive collisions with two neutral species, influence the S^{2+} reactivity we observe. An electric field is applied across the TOF-MS source when the dication pulse reaches the centre of this region. This electric field accelerates positively charged species into the second electric field (acceleration region) of the TOF-MS and then on into the flight tube. At the end of the flight tube, the cations are detected by the position-sensitive detector which comprises a chevron-pair of microchannel plates (diameter = 12.7 cm) located in front of a dual delay-line anode.[98] The voltage pulse applied to the source region also starts the ion timing circuitry, to which the signals from the detector provide stop pulses. The experiments in this work employed TOF-MS source fields of 183 V cm^{-1}. The electrostatic fields employed in the TOF region are homogeneous in order to achieve high mass resolution, therefore our PSCO technique is distinct from 'velocity map imaging'.

Signals from the detector are amplified and discriminated before being passed to a PC-based time-to-digital converter. If two ions are observed in the same TOF cycle, a coincidence event is recorded and each ion's arrival time and impact position on the detector are stored for off-line analysis. The use of single-collision conditions ensures 'false' coincidences are kept to a minimum in our spectra. The ion pairs data can be plotted as a 2D histogram, a 'pairs spectrum', where the time of flights (t_1, t_2) of each ion in the pair are used as the (x, y) co-ordinates. Peaks in the pairs spectrum readily identify bimolecular reaction channels that form a pair of positively-charged product ions. The subset of events associated with each such peak, events corresponding to an individual reaction channel, can then be selected for further off-line analysis.

As shown in previous work, the positional and time of flight information for each ion of a pair can be used to generate their x, y and z velocity vectors in the laboratory frame; here the z-axis is defined by the principal axis of the TOF-MS.[98] The x and y velocity vectors of an ion are determined from the positional information and flight time; the z vector is determined from the deviation of the observed TOF from the expected TOF of an identical ion with zero initial kinetic energy. The laboratory frame velocities are then converted into the CM frame using the initial dication velocity.[98] Often the pair of monocations resulting from the reaction between a dication and a neutral are accompanied by a neutral species: a three-body reaction. A powerful feature of the PSCO-MS experiment is that the CM velocity of such a neutral product can be determined from the CM velocities of the detected ionic products *via* conservation of momentum.[98]

To reveal the dynamics of a given reaction channel, a CM scattering diagram (Fig. 1) can be generated from the velocities of the product ions. Such CM scattering diagrams are radial histograms that, for each event collected for a given reaction channel, plot the magnitude of the products' CM velocity $|w_i|$ as the radial co-ordinate and the scattering angle θ between w_i and the CM velocity of the incident dication as the angular coordinate. In the kinematics that apply in our experiment, where the dication has significantly more momentum than the neutrals, the velocity of the incident dication is closely oriented with the velocity of the centre of mass. In our CM scattering diagrams, since $0^\circ \leq \theta \leq 180^\circ$, the data for one product can be shown in the upper semi-circle of the figure and the data for another

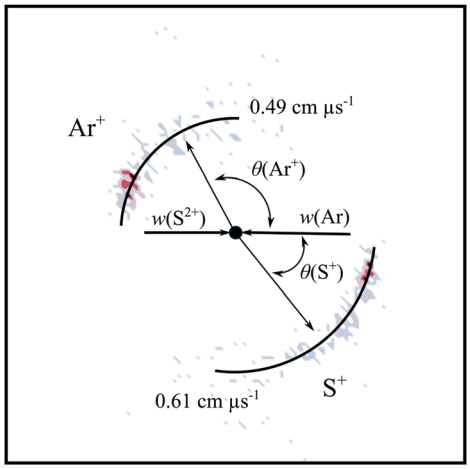

Fig. 1 CM scattering diagram for the reaction S^{2+} + Ar → S^+ + Ar^+ at a CM collision energy of 5.3 eV. The black dot indicates the position of the CM. The intensity scale is logarithmic. See text for details.

Open Access Article. Published on 22 March 2022. Downloaded on 2/21/2026 4:14:56 PM.
This article is licensed under a Creative Commons Attribution 3.0 Unported Licence.

product in the lower semi-circle, as the scattering of each ion is azimuthally symmetric. The typical angular resolution of the scattering data achieved by the PSCO apparatus operating with a high source field is 4°.[69] It should be noted that in our data treatment, to enable presentation in a two-dimensional figure on the page, we are integrating over the azimuthal angle (in which the scattering is cylindrically symmetric). That is, we are binning events according to their value of θ irrespective of the azimuthal scattering angle. This integration over the azimuthal angle results in an isotropic scattering distribution giving a $\sin(\theta)$ intensity distribution in our scattering diagrams, giving our experimental arrangement a lower relative detection efficiency at values of θ very close to 0° or 180°. This phenomenon is ubiquitous where integration over the azimuthal angle occurs and is clearly visible in the scattering diagrams, where even strongly forward scattered reactions exhibit a peak in θ away from $\theta = 0$.

In all the scattering diagrams presented in this work, a logarithmic scale is used for the scattering intensity. Such scales allow the diagrams to reveal subtleties of the low intensity scattering. However, we should be aware that such logarithmic scales can, at first glance, overemphasise the importance of the areas in the scattering diagrams with low intensities. In the ESI† (Fig. SI 1) we contrast scattering diagrams with linear and logarithmic intensity scales.

For three-body reactions, internal-frame scattering diagrams can be a powerful aid in interpreting the reaction dynamics. In this class of scattering diagram $|w_i|$ is again the radial coordinate, but the angular coordinate is now the CM scattering angle with respect to CM velocity of one of the other product species.

From the CM velocities of the product species the total kinetic energy release (KER) T for a given reactive event can also be determined using the individual CM velocities of the products.[98] The exoergicity of the reaction ΔE can then be determined from T and the CM collision energy, E_{com}:

$$\Delta E = T - E_{com} = -(E_{products} - E_{reactants}) \quad (1)$$

where $E_{products}$ and $E_{reactants}$ are the relative energies of the product and reactant states respectively. If the products lie lower in energy than the reactants, the resulting exoergicity will be positive. Performing this analysis for all the events collected for a given reaction channel provides a histogram of the experimental exoergicities of the detected reactive events (*e.g.* Fig. 2). Given knowledge of the available electronic states of the reactants and products, the experimental exoergicity spectrum can reveal the electronic states involved in the reaction. Previous work has shown that such experimental exoergicity spectra can clearly resolve states separated by 1 eV.[102]

To interpret the experimental exoergicity spectra presented below we need to consider the electronic states of S^{2+} populated in our dication beam. Beams of S^{2+} ions generated by EI are not well characterised, but electronic state information is, of course, available for the S^{2+} dication from atomic spectroscopy.[103,104] Experiments studying the electron ionization of H_2S have previously reported the formation of S^{2+}, but provide little information on the S^{2+} states populated.[100,105,106]

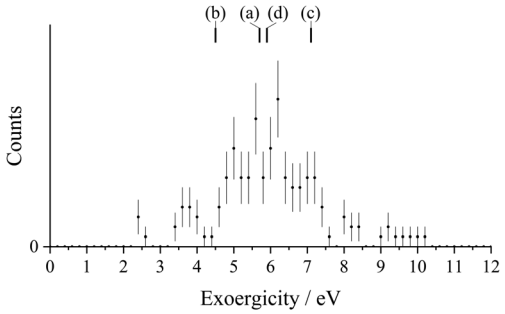

Fig. 2 Experimental exoergicity spectrum for the reaction S^{2+} + Ar → S^+ + Ar^+. Calculated literature exoergicities for the potential SET pathways are also shown (pathways (a)–(d), discussed in the text). The error bars represent two standard deviations of the associated counts.

In our experiments, after the formation of S^{2+} from H_2S *via* electron ionization in the source region, the S^{2+} dications must travel through the apparatus to the interaction region where they can collide with the appropriate neutral species. In the time taken to travel to the interaction region (~100 μs), one would expect S^{2+} formed in higher lying excited states to radiatively decay to lower energy, metastable, states, where such a decay is 'allowed'. Hence, it seems reasonable that the S^{2+} ions in our beam predominantly exist in one of the $[Ne]3s^23p^2$ states (^3P, ^1D or ^1S) from the ground configuration. Such a deduction is in strong accord with experimental determination of the dication states populated when generating the analogous (p^4) states of rare gas dications.[107] Here, electronic states from the ground configuration dominate the dication beam, with the associated electronic states having populations approximately in accord with their degeneracy $9[^3P]:5[^1D]:1[^1S]$.

Ground state $S^{2+}(^3P)$ has an energy of 33.7 eV relative to a neutral S atom in its ground (^1S) state. The excited ^1D and ^1S states lie 35.1 and 37.1 eV above the ground state of S respectively. S^{2+} also has some higher energy states which are potentially long-lived and could therefore also be present in our dication beam: the ^5S state derived from the $[Ne]3s^13p^3$ configuration, which lies 41.0 eV above the ground state of S, and the ^3F state, derived from the $[Ne]3s^23p^13d^1$ configuration, lies 48.8 eV above the ground state of S. Emission lines attributed to decay from the ^5S state of S^{2+} have been observed experimentally, including in the atmosphere Io.[108–110] These investigations reveal the ^5S state is metastable, with estimated lifetimes on the order of ~100 μs, and therefore is possibly a minority species in our S^{2+} beam.[111] The ^3F state has a shorter lifetime than ^5S, but could also be present in the dication beam.[103,111] Given the above, and also noting that the cross section for formation of the various S^{2+} electronic states will increase with excess energy in this ionizing energy regime favouring the population of the p^2 states, we expect our dication beam to be dominated by ions in the ground ^3P state (60%) with the next most abundant state ^1D (30%), with minor contribution (10%) from the ^1S state. Small quantities of the excited ^5S and ^3F states may be present, but likely with a markedly lower abundance than the ^1S state. We will see below that our

Open Access Article. Published on 22 March 2022. Downloaded on 2/21/2026 4:14:56 PM.
This article is licensed under a Creative Commons Attribution 3.0 Unported Licence.

experimental exoergicity spectra strongly support this deduced beam composition, with literature exoergicities associated with reactions of the ^{3}P state accounting for the only observed reaction with Ar, the dominant reaction with H_2 and 98% of the product flux with N_2.

Results and discussion

The collisions of S^{2+} with Ar

PSCO-MS spectra were recorded following the collisions of S^{2+} with Ar at E_{cm} = 5.3 eV. As with all reactions of S^{2+}, there is no prior literature with which to compare our results. The only peak in the coincidence pairs spectrum, $S^+ + Ar^+$, results from single electron-transfer (SET). Fig. 1 shows the scattering of the S^+ and Ar^+ product ions from this SET reaction, revealing strong 'forward' scattering, where the velocity of the S^+ product is oriented in the same direction as the velocity of the reactant dication, $w(S^{2+})$. This forward scattering has been commonly observed for other dicationic SET processes and arises from a direct electron-transfer, where the electron is transferred at a significant interspecies separation (3–6 Å, the so-called reaction window). Such processes are typically well described, for a wide range of collision partners by a Landau–Zener (LZ) formalism.[69,99,112,113] This LZ approach, and the general applicability of the concept of the reaction window, has been established by studies involving a wide range of different ions and targets.[112,114]

Fig. 2 shows a histogram of the event exoergicities recorded in this SET channel. The bulk of the structure in this spectrum is between 4.8 eV and 7.2 eV. In order to interpret the experimental exoergicity distribution, we must consider the possible reactant and product electronic states involved. We discussed above the fact our beam is primarily composed of dications in the p^2 configuration, and likely dominated by the ground $S^{2+}(^3P)$ state. It should be noted that in dication-neutral reactions, in this energy regime, the collision energy (E_{cm}) generally does not couple efficiently to the potential energy surface.[15,112] Therefore, E_{cm} does not usually need to be included when considering the energetics of these reactions. In the ESI,† we present in detail the accessible reactant and product states for this reaction and their associated literature exoergicities, a significant number of which lie in the reaction window (2–7 eV). However, given the arguments above, we see that pathways (a)–(d) of the ^{3}P and ^{1}D states of S^{2+} populating the ground state of Ar^+ and the ground and first excited states of S^+, correlate well with the experimental exoergicity distribution (Fig. 2). These dication states are expected to dominate our beam and the product states involved are readily accessible. Thus, pathways (a)–(d) contributing the bulk of the signals seems highly probable.

Pathways (a)–(d) are all spin allowed and their resulting literature exoergicities are marked in Fig. 2. The range of experimental exoergicities observed in this channel is typical for a LZ governed process (2–7 eV).[112,114]

$$S^{2+}(^3P) + Ar(^1S) \rightarrow Ar^+(^2P) + S^+(^2D) \quad \Delta E = 5.7 \text{ eV} \quad (a)$$

$$S^{2+}(^3P) + Ar(^1S) \rightarrow Ar^+(^2P) + S^+(^2P) \quad \Delta E = 4.5 \text{ eV} \quad (b)$$

$$S^{2+}(^1D) + Ar(^1S) \rightarrow Ar^+(^2P) + S^+(^2D) \quad \Delta E = 7.1 \text{ eV} \quad (c)$$

$$S^{2+}(^1D) + Ar(^1S) \rightarrow Ar^+(^2P) + S^+(^2P) \quad \Delta E = 5.9 \text{ eV} \quad (d)$$

In summary, the above analysis shows that reactions between S^{2+} and Ar are dominated by single electron-transfer with dynamics and energetics that conform well with the established models of dicationic electron transfer. The exoergicities observed support the arguments that our S^{2+} beam is primarily composed of ions from the ground (p^2) configuration. Of course, small contributions from the higher excited states of S^{2+} may be present but would be swamped by the signals from the ^{3}P and ^{1}D states.

The collisions of S^{2+} with H_2

PSCO-MS spectra were recorded following the collisions of S^{2+} and H_2 at E_{cm} = 0.71 eV. Two reaction channels were observed in the coincidence pairs spectrum (Table 1). The dominant channel, Rxn I, is non-dissociative single electron-transfer (NDSET), producing $S^+ + H_2^+$. A dissociative single electron-transfer (DSET) reaction is also observed (Rxn II), resulting in the formation of $S^+ + H^+ + H$. We note, in passing, that the pairs count rate for the S^{2+}/H_2 collision system was markedly lower than the experiments involving Ar or N_2.

There is no peak in the coincidence spectrum resulting from the transfer of two electrons from H_2 to S^{2+}, resulting in the formation of $H^+ + H^+$. Previous work has shown that in dication-neutral systems, facile double electron-transfer (DET) involves a concerted mechanism in which the reactant and product asymptotes have to lie close in energy (<1 eV).[115] Whilst the recombination energy from S^{2+} gaining two electrons is enough (>31.7 eV) to form $H^+ + H^+$ sequentially from H_2, the (vertical) double ionization potential of H_2 is $\sim$51 eV, significantly higher in energy than is accessible from even the ^{3}F state of S^{2+}.[103,116] Therefore, we would not expect the $S^{2+} + H_2$ collisions in our experiment to result in DET *via* a concerted mechanism, in agreement with the experimental data. Hence, the absence of a DET channel in this collision system, despite the accessibility of a step-wise mechanism, adds to the increasing evidence that, in dication-neutral systems, DET reactions occur *via* a concerted two-electron transfer.[115]

Table 1 Reaction channels following the collisions of S^{2+} with H_2 at a CM collision energy of 0.71 eV, with relative intensities. The value of the mode of the experimental exoergicity distribution (ΔE) is reported for each reaction

Reaction	Products	Relative intensity/%	Modal experimental ΔE/eV
I	$S^+ + H_2^+$	61	5.6
II	$S^+ + H^+ + H$	39	12.0

Open Access Article. Published on 22 March 2022. Downloaded on 2/21/2026 4:14:56 PM.
This article is licensed under a Creative Commons Attribution 3.0 Unported Licence.

We note that there is no peak in the coincidence spectrum corresponding to $SH^+ + H^+$, the products of a bond-forming reaction. SH^+ is observed in star-forming regions[117] and diffuse interstellar clouds where it is thought to be involved in ion-neutral chemistry resulting in the formation of a range of sulfur containing species.[118] The formation of $SH^+ + H^+$ from $S^{2+} + H_2$ is exothermic by $\sim$9 eV, therefore we might expect to observe $SH^+ + H^+$ in our experiment,[103,119,120] especially considering the ubiquity of the S–H bond in biological systems, and the propensity of dication + H_2 reactions to result in bond-formation.[17,82–89] The fact we do not observe the formation of $SH^+ + H^+$ could be because in order to transition to the $SH^+ + H^+$ asymptote, the $S^{2+} + H_2$ system has to traverse a region of the potential energy surface with ready access to SET channels. Indeed, the model developed by Herman *et al.*,[86] to explain the competition between SET and bond-forming reactivity in dication-neutral collision systems, shows that the presence of favourable curve crossings that result in SET reduce the probability of bond-forming reactions occurring. The fact we do not observe SH^+ following the collisions of S^{2+} with H_2 suggests that this route is unlikely to contribute to the formation of SH^+ observed in astrophysical environments.

Non-dissociative single electron-transfer (NDSET)

The most intense product channel we observe following collisions between S^{2+} and H_2 is NDSET, forming S^+ and H_2^+. Fig. 3 shows the CM scattering of the S^+ and H_2^+ products in this NDSET channel. It should be noted that because the H_2^+ is significantly lighter than the S^+ fragment, it carries away a large part of the energy release, and the low S^+ velocity leads to increased uncertainty in the scattering angles and velocity of the S^+ product. Fig. 3 shows that the velocity of the S^+ product ion is broadly oriented with the velocity of the incident dication, $w(S^{2+})$. Conversely, the scattering of the H_2^+ product ion is broadly oriented with $w(H_2)$, anti-parallel to $w(S^{2+})$. This form of scattering was also noted in the S^{2+} + Ar SET reaction, and, as mentioned in the discussion of that channel, such kinematics are consistent with direct electron-transfer occurring at a significant interspecies separation (3–6 Å). Such scattering patterns are commonly observed for other NDSET processes and are generally well represented by a LZ formalism.[69,99,112,113]

The experimental exoergicity distribution of this NDSET channel, shown in Fig. 4, is centred at $\sim$6.7 eV, with a full width at half maximum (FWHM) from 4.8–8.6 eV. To rationalise the experimental exoergicity spectrum in this NDSET reaction we must again consider the possible electronic states of the reactant and product species. For this collision system, energetic data are readily available. Given the evidence from the S^{2+} + Ar reaction, and the arguments presented in the experimental section, we would expect the reactions to involve S^{2+} in the $3s^2\ 3p^2$ states.[103] The H_2, emitted as an effusive beam, will be in its ground vibronic state, $X^1\Sigma_g^+\ v = 0$. The ground state of H_2^+ ($X^2\Sigma_g^+$) lies $\sim$15.4 eV in energy above $H_2(X^1\Sigma_g^+)$.[121–123] The lowest energy dissociation asymptote of H_2^+, the energy at which H_2^+ can dissociate and form H^+ + H, is at $\sim$18.1 eV.[124,125] If H_2^+ is formed with energy above this dissociation asymptote it is expected to dissociate within the timescale of our experiment.[121] Therefore, H_2^+ formed above 18.1 eV would not contribute to the H_2^+ counts in this NDSET channel. Photoelectron spectra show that formation of $H_2^+(X^2\Sigma_g^+)$ from the neutral moelcule involves populating vibrational states up to the dissociation asymptote at $\sim$18.1 eV.[126,127] There are also metastable electronic excited states of H_2^+ to consider; however experimental data here are limited.[128] For example, there are three bound vibrational levels of $H_2^+(A^2\Sigma_u^+)$, lying at $\sim$18 eV above the ground state of neutral H_2, just below the H^+ + H dissociation asymptote. However, the large equilibrium internuclear separation means that $H_2^+(A^2\Sigma_u^+)$ is not directly accessible from the H_2 ground state.[129,130] There are also the B and C states of H_2^+, with energies of $\sim$27.1 eV and $\sim$28.2 eV above H_2.[103] These excited states of H_2^+ are not well characterised, as they cannot be accessed by traditional PES. However, any involvement of these excited electronic states of H_2^+ would require a two-electron transition from $H_2(X^1\Sigma_g^+)$ and, in dication + neutral collision systems, ET processes involving the movement of two electrons

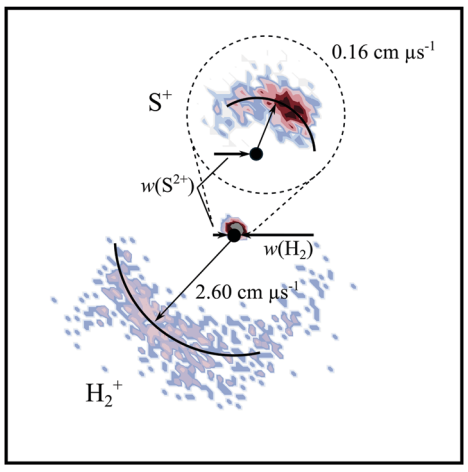

Fig. 3 CM scattering diagram for the reaction $S^{2+} + H_2 \rightarrow S^+ + H_2^+$ at a CM collision energy of 0.71 eV. The scattering of the S^+ product ion is enlarged. The black dot indicates the position of the CM. The intensity scale is logarithmic. See text for details.

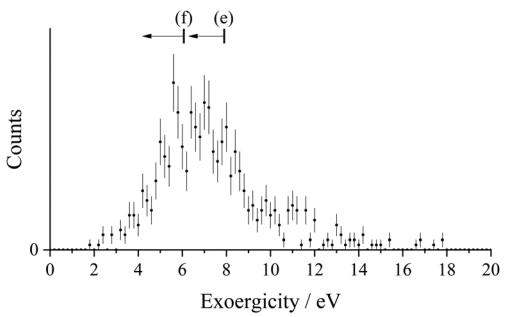

Fig. 4 Experimental exoergicity spectrum for the reaction $S^{2+} + H_2 \rightarrow S^+ + H_2^+$. The error bars represent two standard deviations of the associated counts. The NDSET pathways indicated ((e) and (f)) are discussed in the text and the arrows on the labels indicate the direction of the expected broadening upon population of excited vibrational states of H_2^+.

This journal is © the Owner Societies 2022

Open Access Article. Published on 22 March 2022. Downloaded on 2/21/2026 4:14:56 PM.
This article is licensed under a Creative Commons Attribution 3.0 Unported Licence.

are seen to be significantly less favoured.[131] Therefore, the involvement of excited electronic H_2^+ states in this channel is unlikely.

From energetic considerations, we see that there are many possible reaction pathways that result in literature exoergicities that fall within the range of the observed experimental exoergicities. The reactant dication, S^{2+}, could be in any of the S^{2+} $3s^2$ $3p^2$ electronic states (^{3}P, ^{1}D and ^{1}S). The H_2^+ product ion can be formed in ground state, $X^2\Sigma_g^+$, with a wide range of vibrational excitation: with an energy of anywhere from 15.4 eV ($X^2\Sigma_g^+$ $v = 0$) to the dissociation limit at $\sim$18.1 eV relative to $H_2(X^1\Sigma_g^+)$. The S^+ product ion can be formed in its three lowest energy states: ^{4}S, ^{2}D and ^{2}P.

Previous studies have shown that the vibrational state distribution of product molecular monocations, formed in dication-neutral SET reactions, are dominated by vertical (Frank–Condon style) transitions from the relevant reactant (dication or neutral molecule).[93] Photoelectron spectra of H_2 show that H_2^+ is primarily populated from H_2 with an energy of $< \sim$17.5 eV with respect to the neutral ground state, and it is likely that the H_2^+ formed from H_2 in this NDSET channel will also be formed in this energy range.[121,122,126,127] Given this H_2^+ energy range, and the likely dominance of $S^{2+}(^3P)$ states in the beam, we propose that pathways (e) and (f) involving the ^{3}P state are primarily involved in this NDSET channel. The listed literature exoergicities for these pathways assume the population of $H_2^+(^2\Sigma_g^+)$ $v = 0$. However, as noted above, it is likely that a spread of H_2^+ vibrational states will be formed. The population of excited vibrational levels of H_2^+ will, of course, spread the observed experimental exoergicity to lower values. The literature exoergicities resulting from pathways (e) and (f) are marked on Fig. 4, with arrows showing the energy spread due to the potential vibrational excitation of H_2^+, and provide a good match to the observed experimental exoergicity distribution (Fig. 4). Of course, analogous channels associated with the other states (^{1}D,^{1}S) from the $3p^2$ configuration of S^{2+}, which we expect to be minor components in the S^{2+} beam are also likely to contribute here. Indeed, analogous channels to (e) and (f) for these S^{2+} excited states nicely account for the lower intensity signals up to 11.3 eV in the experimental exoergicity spectrum. However, as for the reaction with Ar, we can easily account for the bulk of the observed exoergicities in terms of the S^{2+} states we argue dominate the dication beam populating readily accessible states of the product ions.

$$S^{2+}(^3P) + H_2(X^1\Sigma_g^+) \rightarrow H_2^+(^2\Sigma_g^+) + S^+(^4S) \quad \Delta E = 7.9 \text{ eV} \tag{e}$$

$$S^{2+}(^3P) + H_2(X^1\Sigma_g^+) \rightarrow H_2^+(^2\Sigma_g^+) + S^+(^2D) \quad \Delta E = 6.1 \text{ eV} \tag{f}$$

Dissociative single electron-transfer (DSET)

The dynamics we extract from each pair of ions making up the $S^+ + H^+$ peak in the coincidence spectrum reveal that the reaction proceeds *via* DSET. The established mechanism for dication + neutral DSET reactions is that an initial LZ style electron-transfer generates one (or both) of the product monocations in a dissociative state.[15] The nascent dissociative states subsequently fragment to yield the observed products. Fig. 5a shows the CM scattering diagram for the S^+ and H^+ products from this DSET channel. As with the NDSET channel discussed above, it should be noted that the relatively low S^+ velocity leads to increased uncertainty in the scattering angles of the S^+. The S^+ is broadly forward scattered but with a tail towards higher angles when compared with the NDSET reaction (Fig. 3), scattering mirrored in the H^+ signals. This scattering pattern is indicative of a longer-lived association between the reactant species than in the standard NDSET process: a $[SH_2]^{2+}$ collision complex. Therefore, this DSET reaction appears not to follow the standard model of dication + neutral electron-transfer where an initial LZ style (long-distance) electron-transfer

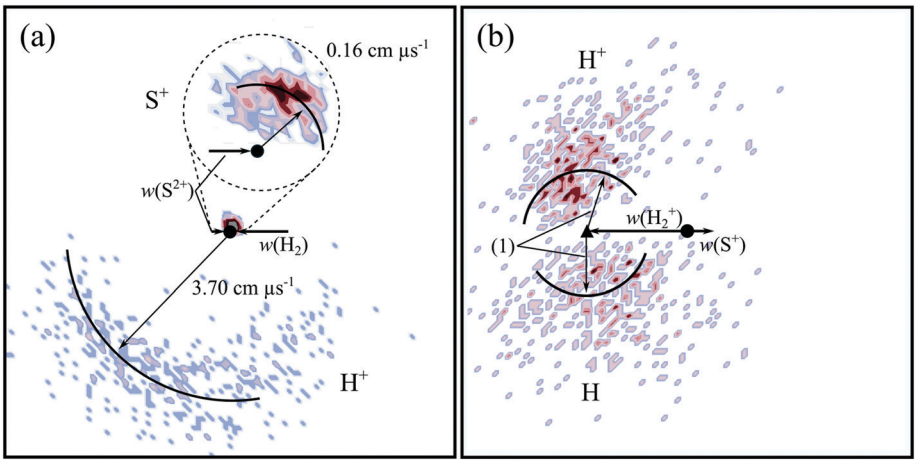

Fig. 5 Scattering diagrams for the DSET reaction $S^{2+} + H_2 \rightarrow S^+ + H^+ + H$ at a CM collision energy of 0.71 eV. The black dot indicates the position of the CM. (a) CM scattering diagram showing the S^+ and H^+ products relative to the incident dication velocity, $w(S^{2+})$. The scattering of the S^+ product ion is enlarged. (b) Internal frame scattering diagram showing the scattering of H^+ and H relative to $w(S^+)$. See the experimental section for the details of these two classes of scattering diagram. The labelled vector (1) = 1.9 cm μs^{-1}. The intensity scale is logarithmic.

Open Access Article. Published on 22 March 2022. Downloaded on 2/21/2026 4:14:56 PM.
This article is licensed under a Creative Commons Attribution 3.0 Unported Licence.

populates one of the products in a dissociative electronic state.[95,132,133] As discussed, such an LZ style electron-transfer reaction should lead to a more prominent forward scattering pattern than is observed here. Indeed, although not common, SET involving complexation has been observed before in dication/neutral reactions.[90,95,132,133] Electron ionization experiments studying H_2S show evidence for H_2S^{2+} states that are energetically accessible to the $S^{2+} + H_2$ reactants in this system, and that dissociate to form $S^+ + H_2^+$.[100] These H_2S^{2+} states could be involved as a short-lived intermediates in this DSET channel.

Fig. 5b shows the scattering of the H^+ and H fragments relative to the velocity of the S^+ product ion. We refer the reader back to Section 3 for information on the construction of these internal frame scattering diagrams. The H^+ and H fragments are both clearly backward scattered, away from the S^+ ion and their scattering is distributed about a clear H_2^{+*} precursor velocity which is indicated in Fig. 5b. This scattering motif, which has been observed before for many DSET reactions,[112,114,115,134] clearly shows the $[SH_2]^{2+}$ complex dissociates into $S^+ + H_2^{+*}$ before the fragmentation of H_2^{+*}. The H^+ fragment ion distribution is slightly more energetically backward scattered than that of the H fragment, likely because the H_2^{+*} ion fragments within the electric field of the S^+ ion, resulting in the H^+ experiencing an additional acceleration.

The experimental exoergicity observed from this DSET channel is shown in Fig. 6. The experimental exoergicity distribution has a broad maximum, centred at ~10 eV, with a FWHM from 6.5–15.5 eV. In order to give the exoergicities observed in this channel, the S^{2+} dication must be in an electronically excited state, thus the dominant species we expect in the dication beam $S^{2+}(^3P)$ cannot contribute and the experimental exoergicity spectrum reveals the excited S^{2+} states in the beam. Even the coupling of the collision energy (0.71 eV) into the energetics does not allow reactions of $S^{2+}(^3P)$ to generate the observed exoergicities. Representative reactions of the relevant S^{2+} excited states (g)–(j) which fit the observed experimental exoergicity distribution are given below. Variations on these processes are also compatible with the exoergicity data (Fig. 6) involving, for example, the formation of excited states of S^+. The literature exoergicities resulting from pathways (g)–(j) are marked on the experimental exoergicity spectrum in Fig. 6. There is an exoergic channel for the ^1D state (Fig. 6, (g)), but the maximum exoergicity possible for the highest energy state of the p^2 configuration (^1S) is 8.6 eV (marked by (h) in Fig. 6) and there are clearly events with experimental exoergicities markedly above this value; such exoergicities can only be generated by electronic states of S^{2+} from excited configurations. That is, the demanding energetics allow the contribution of these minor beam components to be distinguished from that of the p^2 configuration. Above we considered a minor beam component as comprising the metastable ^5S and ^3F states. Reaction of $S^{2+}(^5S)$ can give exoergicities up to ~12.5 eV, and the involvement of ^3F can give exoergicities of up to ~20.4 eV. These exoergicities nicely encompass the higher end of the observed experimental exoergicity distribution (Fig. 6, (i)–(j)) and indeed the reaction of the ^3F state correlates nicely with a weak high exoergicity feature in the spectrum (Fig. 6, (j)).

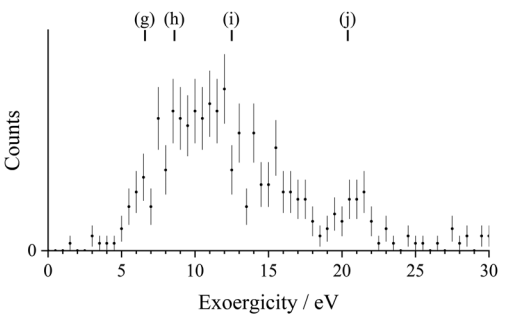

Fig. 6 Experimental exoergicity spectrum for the reaction $S^{2+} + H_2 \rightarrow S^+ + H^+ + H$. The error bars represent two standard deviations of the associated counts.

Despite the assignments of the product states not being definitive, it is clear that the DSET reaction with H_2 involves the excited states of S^{2+} we predicted to be present in the dication beam. The contribution of these excited states dominates the product flux in this reaction channel as the demanding energetics mean the dominant dication state in the ion beam, the ^3P ground state of S^{2+}, cannot contribute. Given our deductions concerning the dominance of the ^3P state in the beam, the involvement of excited S^{2+} in this channel explains the low signal rate noted above.

$$S^{2+}(^1D) + H_2(X^1\Sigma g^+) \rightarrow S^+(^4S) + H(^2S) + H^+ \quad \Delta E = 6.6 \text{ eV} \quad \text{(g)}$$

$$S^{2+}(^1S) + H_2(X^1\Sigma g^+) \rightarrow S^+(^4S) + H(^2S) + H^+ \quad \Delta E = 8.6 \text{ eV} \quad \text{(h)}$$

$$S^{2+}(^5S) + H_2(X^1\Sigma g^+) \rightarrow S^+(^4S) + H(^2S) + H^+ \quad \Delta E = 12.5 \text{ eV} \quad \text{(i)}$$

$$S^{2+}(^3F) + H_2(X^{1-}\Sigma g^+) \rightarrow S^+(^4S) + H(^2S) + H^+ \quad \Delta E = 20.4 \text{ eV} \quad \text{(j)}$$

Applying a powerful approach we have used in previous work to study the energetics of DSET reactions we can, on an event-by-event basis, determine the velocity of the precursor H_2^{+*} ion from the measured velocity of the S^+ ion using conservation of momentum. The S^+ and H_2^{+*} velocities then allow us to construct an exoergicity spectrum for the initial electron transfer step to reveal the electronic states involved. Subsequently, again on an event by event basis we can examine the velocities of the H and H^+ products in the frame of the H_2^{+*} precursor velocity to derive a spectrum representing the energies involved in the dissociation of the H_2^{+*} ion. This analysis assumes the formation of $S^+ + H_2^{+*}$ can be treated as a two-body reaction, dynamically distinct from the subsequent dissociation of the H_2^{+*}. Given the observed scattering dynamics (Fig. 5b) this is clearly a good, but not perfect approximation. Applying this approach yields the experimental

 This journal is © the Owner Societies 2022

Open Access Article. Published on 22 March 2022. Downloaded on 2/21/2026 4:14:56 PM.
This article is licensed under a Creative Commons Attribution 3.0 Unported Licence.

exoergicity distribution for dissociation of H_2^{+*} to $H^+ + H$ shown in Fig. 7.

In 1986, Cordaro *et al.*[125] studied the dissociation of H_2^+ generated by electron ionization, observing experimental exoergicities from 2–8 eV. Strathdee and Browning[135] observed similar kinetic energy releases, ranging from 4–10 eV, using 26.9 eV photoionization. In their study of H_2 electron ionization, Köllmann[136] reported H^+ kinetic energy distributions that correspond to kinetic energy releases ranging from 0–24 eV resulting from H_2^+ dissociation. The electronic states attributed to these kinetic energy releases were the high vibrational states of $H_2^+(X^2\Sigma_g^+)$ and $H_2^+(A^2\Sigma_u^+)$. Other experiments studying photo- and electron-ionization of H_2 also resulted in the observation of kinetic energy releases from H_2^+ dissociation of up to ~20 eV.[137–139] The bulk of the experimental exoergicity distribution resulting from H_2^+ dissociation observed in our experiment (Fig. 7) matches well with Cordaro *et al.*[125] and Strathdee and Browning,[135] and the shoulder towards higher experimental exoergicities is in agreement with the distributions observed by Köllmann and others.[136–139] The agreement between the exoergicity release resulting from H_2^+ dissociation observed in our experiment and those previously reported confirms that the mechanism responsible for the formation of $S^+ + H^+$ in this channel is DSET *via* H_2^{+*}.

As mentioned, if H_2^+ is formed at energies over ~18.1 eV above the ground state of the neutral H_2 molecule, it will dissociate.[124,125] Our analysis of the experimental exoergicity (Fig. 6) above suggests that only the lowest energy H state (^{2}S) is formed in this dissociation. To yield experimental exoergicities in the range observed in Figure 7, H_2^+ therefore needs to be primarily formed with energies between 19–24 eV relative to $H_2(X^1\Sigma_g^+)$. Thus, the H_2^+ ion could be populated in the $A^2\Sigma_u^+$ state. As noted above, the geometry of the $A^2\Sigma_u^+$ state in the 19–24 eV energy range is significantly different to the neutral molecule and would therefore not be expected to be efficiently formed in a vertical ionizing transition. Moreover, the formation of $H_2^+(A^2\Sigma_u^+)$ from $H_2(X^1\Sigma_g^+)$ is a two-electron transition, which, as discussed above, is thought to be significantly less likely than a one-electron process.[131] However, both forming the H_2^+ ion with a markedly different geometry to the neutral species, and the movement of two electrons are more feasible if the reaction proceeds *via* a collision complex, as suggested by the scattering we observe. Alternatively, H_2^+ could be formed in the continuum of the $X^2\Sigma_g^+$ state, above the 18.1 eV dissociation asymptote. The involement of either the $H_2^+(A^2\Sigma_u^+)$ or $H_2^+(X^2\Sigma_g^+)$ states is in good agreement with the H_2^+ dissociation studies discussed above.[125,136]

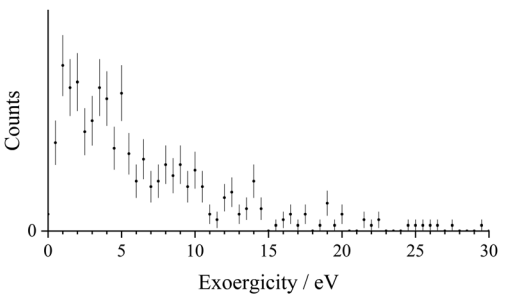

Fig. 7 Experimental exoergicity spectrum for the dissociation of H_2^+ to form $H^+ + H$. The H_2^+ is formed *via* the initial electron-transfer reaction $S^{2+} + H_2 \rightarrow S^+ + H_2^+$. The error bars represent two standard deviations of the counts. See text for details.

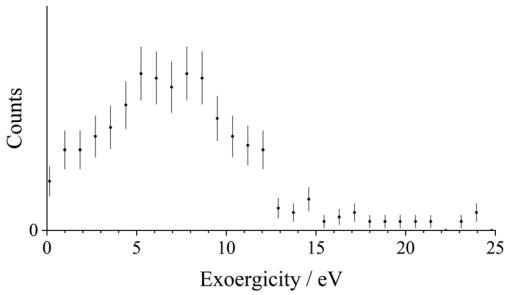

Fig. 8 Experimental exoergicity spectrum determined from precursor velocities for the initial electron-transfer reaction in the DSET channel, $S^{2+} + H_2 \rightarrow S^+ + H_2^{+*}$ [$\rightarrow S^+ + H^+ + H$]. The error bars represent two standard deviations of the associated counts. See text for details.

As discussed above, the exoergicity of the initial electron-transfer step of this DSET reaction can also be evaluated using the precursor velocity of the H_2^+ ion and $w(S^+)$. Using this method, an estimate of the experimental exoergicity distribution for the initial electron-transfer step ($S^{2+} + H_2 \rightarrow S^+ + H_2^{+*}$) was determined and is shown in Fig. 8. The experimental exoergicity distribution has a broad peak centred at ~7 eV with a FWHM from 1–12 eV. The observed experimental exoergicity distribution exceeds the typical range for LZ style processes (2–7 eV),[112,114] providing further indirect evidence that this DSET reaction proceeds *via* a collision complex, as suggested by the scattering.

The experimental exoergicity distribution determined for the initial electron-transfer step (Fig. 8) aligns satisfyingly with the literature exoergicities expected from our above assessment of the likely electronic states involved in this channel. These include the excited states of S^{2+} (^{1}D, ^{1}S, ^{5}S and ^{3}F), the lowest three energy states of S^+ (^{4}S, ^{2}D and ^{2}P), and $H_2^+(A^2\Sigma_u^+)$ or the continuum of the $H_2^+(X^2\Sigma_g^+)$ state. The possible involvement of this large number of states, and the range of vibrational excitation available for H_2^+, results in too many accessible pathways to determine which specific states are involved.

In summary, DSET occurs following the collisions of $S^{2+} + H_2$, resulting in the formation of $S^+ + H^+$ (+ H). This channel involves S^{2+} in its electronically excited states derived from the $3s^23p^2$ electron configuration (^{1}D, ^{1}S) and also shows evidence for the presence of higher energy S^{2+} states in the beam: ^{5}S and ^{3}F, resulting from the $3s^13p^3$ and $3s^23p^13d^1$ configurations respectively. This DSET channel involves the formation of S^+ primarily in its lowest electronic state (^{4}S), with contributions from the first two excited states, ^{2}D and ^{2}P. The nascent H_2^+ ion is generated at initial energies of between 19 eV and 24 eV relative to $H_2(X^1\Sigma_g^+)$ before dissociating to the lowest energy asymptote: $H^+ + H(^2S)$.

Open Access Article. Published on 22 March 2022. Downloaded on 2/21/2026 4:14:56 PM.
This article is licensed under a Creative Commons Attribution 3.0 Unported Licence.

The collisions of S^{2+} + N_2

PSCO-MS spectra were recorded following the collisions of S^{2+} and N_2 at E_{cm} = 4.7 eV. In the coincidence pairs spectrum three reaction channels which produce pairs of product ions were observed, and are shown in Table 2. The dominant channel, Rxn III, is NDSET, producing $S^+ + N_2^+$. A DSET reaction (Rxn IV), results in the formation of $S^+ + N^+ + N$. Finally, a bond-forming channel (Rxn V), producing $SN^+ + N^+$, is detected.

Whilst the PSCO-MS apparatus is optimised for the detection of pairs of ions, we also record a simple mass spectrum of single ion arrivals. We do not detect any structures present in this mass spectrum ions in the m/z = 23 region that could be indicative of SN^{2+} or the m/z = 30 region that could be indicative of SN_2^{2+}. However, we note that the sensitivity of our experiment is optimised for detecting ion pairs involving energetic monocations, not product dications.

It is notable that there is no peak in the coincidence spectrum corresponding to $N^+ + N^+$, the products of a dissociative DET reaction. However, the absence of a DET reaction is not surprising as the polarisability of S (2.9×10^{-24} cm^3) is greater than N_2 (1.7403×10^{-24} cm^3).[140] In this situation, under the concerted model of DET,[115,133] we would not expect the $S^{2+} + N_2$ and $S + N_2^{2+}$ curves to cross even if the $S^{2+} + N_2 \rightarrow S + N_2^{2+}$ reaction was exothermic; this situation has been shown before to strongly disfavour DET. Added to this, DET between S^{2+} and N_2 would be endothermic for S^{2+} states with energies below $S^{2+}(^3F)$, the states that we have deduced make up the bulk of our S^{2+} beam.

Non-dissociative single electron-transfer (NDSET)

Fig. 9 shows the CM scattering diagram for the $S^+ + N_2^+$ product ions of the NDSET reaction, $S^{2+} + N_2 \rightarrow S^+ + N_2^+$. A strong forward scattering pattern is observed, where the S^+ is oriented in the same direction as $w(S^{2+})$, whilst the N_2^+ product is oriented in the same direction as $w(N_2)$. Note the peaking of the signals in Fig. 9 slightly away from θ = 0° and 180° as discussed in the experimental section. This scattering pattern is typical of a direct electron-transfer process, occurring at a relatively large interspecies separation (3–6 Å) as discussed above. These electron-transfer dynamics are well represented by a Landau–Zener formalism.[69,99,112,113]

Fig. 10 shows a histogram for the experimental exoergicities recorded in this NDSET reaction channel. The spectrum shows a structure with a maximum at 5.6 eV, and a FWHM from 4.3–6.9 eV. The observed experimental exoergicities are typical for such a LZ style SET reaction.[112,114] As discussed above, we have good evidence that the dication beam is primarily comprised of S^{2+} in the $3s^23p^2$ configuration, dominated by the ^3P state. The N_2 reactant will be in its ground vibronic state, $X^1\Sigma_g^+$ v = 0. The ground state of N_2^+, $X^2\Sigma_g^+$, has an energy of 15.58 eV relative to $N_2(X^1\Sigma_g^+)$.[141,142] If N_2^+ is formed with energies above ~24.3 eV relative to $N_2(X^1\Sigma_g^+)$ (corresponding to $N_2^+(C^2\Sigma_u^+$ v = 3)), it will be unstable to dissociation to the $N^+(^3P)$ + $N(^4S)$ asymptote.[103,143] Photoionization studies have shown that N_2^+ states generated with more than 24.3 eV, relative to $N_2(X^1\Sigma_g^+)$, have dissociation lifetimes less than the timescale of our experiment. Therefore, we do not expect any contribution to the N_2^+ counts observed in this channel from N_2^+ states formed with more than 24.3 eV of energy with respect to N_2.[143–146] Electron-transfer occurring between N_2 and any of the ^3P, ^1D and ^1S electronic states of S^{2+} can result in the formation of S^+ in any of the states from the ground state (^4S) up to the ^4F state, derived from the [Ne] $3s^2$ $3p^2$ $3d^1$ configuration.

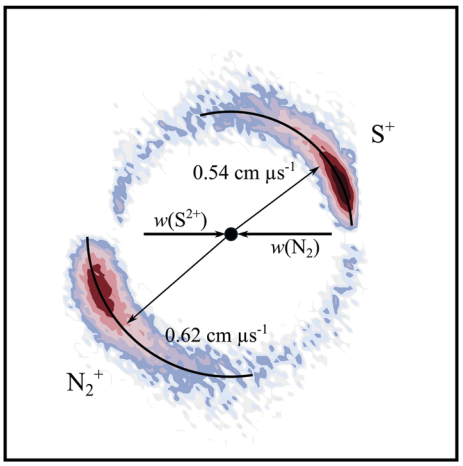

Fig. 9 CM scattering diagram for the reaction $S^{2+} + N_2 \rightarrow S^+ + N_2^+$ at a CM collision energy of 4.7 eV. The black dot indicates the position of the CM. The intensity scale is logarithmic. See text for details.

Table 2 Reaction channels following the collisions of S^{2+} with N_2 at a CM collision energy of 4.7 eV, with relative intensities. The value of the mode of the experimental exoergicity distribution (ΔE) is reported for each reaction

Reaction	Products	Relative intensity/%	Modal experimental ΔE/eV
III	$S^+ + N_2^+$	98	5.6
IV	$S^+ + N^+ + N$	1	—[a]
V	$SN^+ + N^+$	1	2.0

[a] The signal-to-noise ratio in Rxn IV is low and therefore it is difficult to extract meaningful energetic information from this channel.

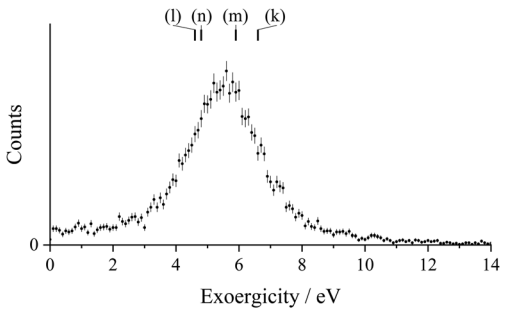

Fig. 10 Experimental exoergicity spectrum for the reaction $S^{2+} + N_2 \rightarrow S^+ + N_2^+$. The error bars represent two standard deviations of the associated counts. The literature exoergicities resulting from the pathways (k)–(n) are indicated. See text for details.

This journal is © the Owner Societies 2022

Open Access Article. Published on 22 March 2022. Downloaded on 2/21/2026 4:14:56 PM.
This article is licensed under a Creative Commons Attribution 3.0 Unported Licence.

Considering the above constraints, we find that there are many possible electronic pathways that could be involved in the formation of $S^+ + N_2^+$. However, as discussed above we expect the major component of our S^{2+} beam to be ions in the ^3P state. Possible pathways involving the ^3P state are shown by (k)–(n), and their resulting literature exoergicities are shown on Fig. 10. These channels show N_2^+ is likely formed in one of the stable $X^2\Sigma_g^+$, $A^2\Pi_u$ or $B^2\Sigma_u^+$ states, which reassuringly are those which dominate photoelectron spectra,[141] and the S^+ products are primarily the lowest two electronic states: ^4S and ^2D. Although these contributions from the dication ^3P state (pathways (k)–(n)) can account for the signals we observe, especially when varying degrees of vibrational excitation of the product N_2^+ ion is considered which will broaden the observed exoergicities, excited S^{2+} states could also be contributing to the product flux in this NDSET channel. However, given energetically favourable channels for the reaction of the ^3P state, which lie in the reaction window, and the expected dominance of this state in the ion beam, we feel confident that pathways (k)–(n) account for the bulk of the events we detect in this reactive channel.

$$S^{2+}(^3P) + N_2(X^1\Sigma g^+) \rightarrow S^+(^4S) + N_2^+(A^2\Pi_u) \quad \Delta E = 6.6 \text{ eV} \quad (k)$$

$$S^{2+}(^3P) + N_2(X^1\Sigma g^+) \rightarrow S^+(^4S) + N_2^+(B^2\Sigma_u^+) \quad \Delta E = 4.6 \text{ eV} \quad (l)$$

$$S^{2+}(^3P) + N_2(X^1\Sigma g^+) \rightarrow S^+(^2D) + N_2^+(X^2\Sigma_g^+) \quad \Delta E = 5.9 \text{ eV} \quad (m)$$

$$S^{2+}(^3P) + N_2(X^1\Sigma g^+) \rightarrow S^+(^2D) + N_2^+(A^2\Pi_u) \quad \Delta E = 4.8 \text{ eV} \quad (n)$$

Dissociative single electron-transfer (DSET)

The peak in the coincidence pairs spectrum corresponding to the detection of ions with $m/z = 32$ and $m/z = 14$ is due to the formation of S^+ and N^+. The peak is weak, so it is only possible to probe the dynamics and exoergicities in an indicative manner. In order to discriminate against some of the stray counts arising from background noise, which become problematic in this channel due to the low number of counts, any events that gave unrealistic experimental exoergicities were removed before the analysis.

Fig. 11a shows the CM scattering diagram for the S^+ and N^+ products resulting from this channel. The S^+ ions are broadly forward scattered, however, there is scattering to higher angles. Conversely, the N^+ ions are broadly backscattered, with some ions scattered towards lower angles. One might expect a higher propensity of forward scattering if this channel resulted from a direct, LZ style electron-transfer. The presence of scattering to higher angles could be evidence of the involvement of a collision complex, however, due to the low intensity signal in this channel, it is difficult to be conclusive. Fig. 11b shows the internal frame scattering of the N^+ and N products relative to the S^+ product ion. The N^+ and N ions are scattered around the expected precursor velocity of an N_2^{+*} intermediate, confirming the mechanism of this channel as DSET. SET occurs, producing N_2^{+*} in a dissociative state (and S^+), which then dissociates to form $N^+ + N$. In Fig. 11b the N^+ is scattered away from the S^+ with a higher velocity than the N fragment. This asymmetric scattering of the N^+ and N fragments is because the N_2^{+*} species dissociates within the electric field of the S^+ ion, and Coulomb repulsion then accelerates only the N^+ species. Such behaviour has been noted before for DSET channels in other dicationic collision systems.[90,115,133]

The experimental exoergicity distribution resulting from this DSET channel reveals a broad structure between 0.5 eV and 11.0 eV. Note that due to the low intensity, the energy resolution is low, and hence any conclusions we draw from this data must be tentative. It is not common to see energy releases of less than 2 eV for reactions involving LZ style ET, however, as discussed above, the scattering hints that a more complicated

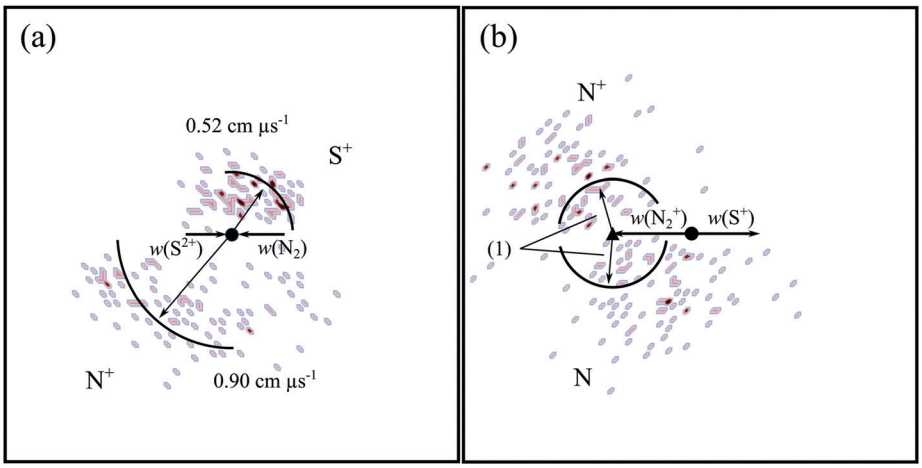

Fig. 11 Scattering diagrams for the DSET reaction $S^{2+} + N_2 \rightarrow S^+ + N^+ + N$ at a CM collision energy of 4.7 eV. The black dot indicates the position of the CM. (a) CM scattering diagram showing the S^+ and N^+ products relative to the incident dication velocity, $w(S^{2+})$. (b) Internal frame scattering diagram showing the scattering of N^+ and N relative to $w(S^+)$. In part (b) the labelled vector, (1), represents 0.44 cm μs^{-1}.

Open Access Article. Published on 22 March 2022. Downloaded on 2/21/2026 4:14:56 PM.
This article is licensed under a Creative Commons Attribution 3.0 Unported Licence.

reaction mechanism is involved. The formation of $N^+ + S^+ + N$ resulting from the ground state of $S^{2+}(^3P)$ is endothermic, therefore the occurrence of this channel again confirms the existence of electronically excited states of S^{2+} in the dication beam. Indeed, the exclusive involvement of higher energy S^{2+} states undoubtedly accounts for the low intensity of this DSET channel. The involvement of $S^{2+}(^1S)$ can result in exoergicities in this DSET channel of up to 2.4 eV, significantly lower than the bulk of the observed experimental exoergicity distribution. However, the involvement of the ^5S and ^3F states of S^{2+} allows events with exoergicities of up to 6.3 eV and 14.1 eV respectively. Given the high experimental exoergicities observed in this DSET channel, the S^+, N^+ and N fragments are likely all formed in their ground or lower energy excited electronic states.

The experimental exoergicity of the N_2^{+*} dissociation, calculated from the N_2^+ precursor velocity, has structure from 0.3–4.0 eV. This range of experimental exoergicities is comparable to those observed from N_2^+ dissociation in the DSET channel in our previous investigation of $Ar^{2+} + N_2$ collisions.[90] As mentioned above, N_2^+ states generated with more than 24.3 eV above $N_2(X^1\Sigma_g^+)$ are unstable to dissociation and will dissociate within the lifetime of our experiment. Considering the experimental exoergicity of the complete reaction and the N_2^+ dissociation exoergicity, N_2^+ is likely formed with energies of 25–29 eV above $N_2(X^1\Sigma_g^+)$ and primarily dissociates to the lowest energy $N^+ + N$ asymptote, with both N^+ and N in their ground electronic states.

Chemical bond-formation

The peak in the pairs spectrum corresponding to the ions m/z = 46 and m/z = 14 is due to the detection of SN^+ and N^+: a bond-forming reaction (Rxn V). The SN^+ molecular ion is relevant to a range of astrophysical environments, including in comets and nebulae.[147–151] SN^+ is also important terrestrially, in man-made plasmas.[152]

Fig. 12 shows the CM scattering for the SN^+ and N^+ product ions in this channel, revealing an isotropic scattering pattern. Such scattering is strong evidence for the involvement of an intermediate, long-lived, collision complex, $[SN_2]^{2+}$. The collision complex exists for at least several rotations, before fragmenting into SN^+ and N^+, as shown in (o).

$$S^{2+} + N_2 \rightarrow [SN_2]^{2+} \rightarrow SN^+ + N^+ \qquad \text{(o)}$$

The experimental exoergicity of Rxn V, determined from the product ion velocities, is shown in Fig. 13. The experimental exoergicity distribution has a maximum at 2.0 eV with a FWHM from 0.5–4.5 eV. In order to rationalise the observed experimental exoergicities, we must again consider the possible electronic states of the reactant and product species. Due to its astrophysical relevance, the SN^+ species has been the subject of experimental study,[150,153,154] and several theoretical investigations have probed the electronic states of SN^+.[151,155–157] In this work we use the electronic state structure calculated by Ben Yaghlane & Hochlaf (2009),[151] as it provides the most

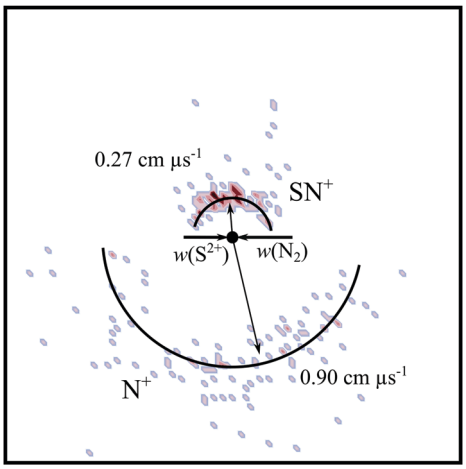

Fig. 12 CM scattering diagram for the reaction $S^{2+} + N_2 \rightarrow SN^+ + N^+$ at a CM collision energy of 4.7 eV. The black dot indicates the position of the CM. See text for details.

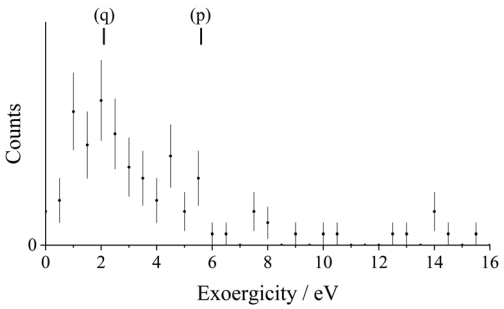

Fig. 13 Experimental exoergicity spectrum for the reaction $S^{2+} + N_2 \rightarrow SN^+ + N^+$. The error bars represent two standard deviations of the associated counts. The literature exoergicities of potential reaction pathways (p) and (q) are indicated. See text for details.

comprehensive data. The SN^+ ground state ($X^1\Sigma^+$) lies ~6.3 eV below the lowest energy dissociation asymptote of $S^+(^4S) + N(^4S)$, and ~8.3 eV below the second lowest energy dissociation asymptote of $S^+(^2D) + N(^4S)$. There are also many other bound SN^+ electronic states lying below these dissociation asymptotes, several with well depths sufficient to sustain vibrational excitation. Again, we assume that the dication beam is primarily comprised of the ground configuration, dominated by the ^3P state, and N_2 is in its ground vibronic state ($^1\Sigma_g^+$). These energetics mean that N^+ can therefore be formed in any of its four lowest energy electronic states.

Considering the above, there are a large number of pathways that match the observed experimental exoergicity distribution of this bond-forming channel. Two likely pathways which match well with the exoergicity spectrum and involve the ground state of S^{2+}, the dominant ion in our beam, are shown by (p) and (q):

$$S^{2+}(^3P) + N_2(^1\Sigma_g^+) \rightarrow SN^+(X^1\Sigma^+) + N^+(^3P) \quad \Delta E = 5.6 \text{ eV} \qquad \text{(p)}$$

$$S^{2+}(^3P) + N_2(^1\Sigma_g^+) \rightarrow SN^+(1^3\Sigma^+) + N^+(^3P) \quad \Delta E = 2.1 \text{ eV} \qquad \text{(q)}$$

This journal is © the Owner Societies 2022

Open Access Article. Published on 22 March 2022. Downloaded on 2/21/2026 4:14:56 PM.
This article is licensed under a Creative Commons Attribution 3.0 Unported Licence.

The ^{1}D and ^{1}S states of S^{2+} could also be involved, as well as the first three excited states of N^+ (^{1}D, ^{1}S and ^{5}S). Moreover, it is possible that a number of the electronic states of SN^+ that are stable to dissociation could be populated in this channel.

To summarise, this channel involves a chemical bond-forming reaction between S^{2+} + N_2, producing SN^+ + N^+. An isotropic scattering pattern is observed, clearly showing the involvement of a collision complex, $[SN_2]^{2+}$, typical for a dicationic bond-forming reaction. The observed experimental exoergicity distribution is in good agreement with the population of known electronic states of SN^+,[151] and the involvement of the S^{2+} states that we know dominate our S^{2+} beam.

Conclusions

In this work we have studied the gas-phase reactivity of S^{2+} with Ar, N_2 and H_2. This, to our knowledge, is the first study of the bimolecular reactivity of S^{2+}. The experiments indicate that the dication beam is composed predominantly of S^{2+} ions resulting from the $3s^23p^2$ ground electronic configuration. Most of the observed reaction channels can be accounted for by the involvement of S^{2+} in its ground state, ^{3}P. However, the dissociative electron transfer reactivity reveals the involvement of higher energy S^{2+} states.

The SET reaction between S^{2+} and Ar displays dynamics and energetics typical of a Landau–Zener style electron transfer reaction. In the reactions between S^{2+} + H_2, NDSET and DSET were observed. The dynamics here show evidence for the formation of a long-lived association between the reactants, a collision complex $[SH_2]^{2+}$. Perhaps surprisingly, the formation of SH^+, the potential product of a chemical bond-forming channel, was not observed. The reactions of S^{2+} + H_2 are especially relevant as S^{2+} has been observed in the outer atmosphere of Jupiter, where H_2 is the dominant chemical species. The collisions of S^{2+} + N_2 result in both dissociative and non-dissociative SET reactions as well as a bond-forming channel, the latter resulting in the formation of SN^+ + N^+. This bond-forming reaction proceeds *via* a collision complex.

Conflicts of interest

There are no conflicts to declare.

Acknowledgements

We gratefully acknowledge the financial support of the EPSRC (EP/J010839/1), the Leverhulme Trust (RPG-2017-309), the Royal Society of Chemistry (E21-4679591105) and UCL.

References

1 C. Simon, J. Lilensten, O. Dutuit, R. Thissen, O. Witasse, C. Alcaraz and H. Soldi-Lose, *Ann. Geophys.*, 2005, **23**, 781–797.
2 H. S. Bridge, J. W. Belcher, A. J. Lazarus, J. D. Sullivan, R. L. McNutt, F. Bagenal, J. D. Scudder, E. C. Sittler, G. L. Siscoe, V. M. Vasyliunas, C. K. Goertz and C. M. Yeates, *Science*, 1979, **204**, 987–991.
3 S. Ghosh, K. K. Mahajan, J. M. Grebowsky and N. Nath, *J. Geophys. Res.*, 1995, **100**, 23983–23991.
4 J. H. Hoffman, C. Y. Johnson, J. C. Holmes and J. M. Young, *J. Geophys. Res.*, 1969, **74**, 6281–6290.
5 E. Dubinin, R. Modolo, M. Fraenz, J. Woch, G. Chanteur, F. Duru, F. Akalin, D. Gurnett, R. Lundin, S. Barabash, J. D. Winningham, R. Frahm, J. J. Plaut and G. Picardi, *J. Geophys. Res.: Space Phys.*, 2008, **113**, A10217.
6 J. Lilensten, O. Witasse, C. Simon, H. Soldi-Lose, O. Dutuit, R. Thissen and C. Alcaraz, *Geophys. Res. Lett.*, 2005, **32**, L03203.
7 J. Lilensten, C. Simon, O. Witasse, O. Dutuit, R. Thissen and C. Alcaraz, *Icarus*, 2005, **174**, 285–288.
8 O. Witasse, O. Dutuit, J. Lilensten, R. Thissen, J. Zabka, C. Alcaraz, P.-L. Blelly, S. W. Bougher, S. Engel, L. H. Andersen and K. Seiersen, *Geophys. Res. Lett.*, 2002, **29**, 104.
9 B. J. Wilkes, G. J. Ferland, D. Hanes and J. W. Truran, *Mon. Not. R. Astron. Soc.*, 1981, **197**, 1–6.
10 D. K. Böhme, *Phys. Chem. Chem. Phys.*, 2011, **13**, 18253–18263.
11 J. P. Simpson, R. H. Rubin, E. F. Erickson and M. R. Haas, *Astrophys. J.*, 1986, **311**, 895–908.
12 R. S. Houk, *Anal. Chem.*, 1980, **52**, 2283–2289.
13 A. Bogaerts and R. Gijbels, *J. Appl. Phys.*, 1999, **86**, 4124–4133.
14 J. S. Becker, G. Seifert, A. I. Saprykin and H.-J. Dietze, *J. Anal. At. Spectrom.*, 1996, **11**, 643–648.
15 S. D. Price, J. D. Fletcher, F. E. Gossan and M. A. Parkes, *Int. Rev. Phys. Chem.*, 2017, **36**, 145–183.
16 D. Ascenzi, J. Aysina, E. L. Zins, D. Schröder, J. Žabka, C. Alcaraz, S. D. Price and J. Roithová, *Phys. Chem. Chem. Phys.*, 2011, **13**, 18330–18338.
17 J. Roithová, H. Schwarz and D. Schröder, *Chem. – Eur. J.*, 2009, **15**, 9995–9999.
18 W. Wolff, H. Luna, R. Schuch, N. D. Cariatore, S. Otranto, F. Turco, D. Fregenal, G. Bernardi and S. Suárez, *Phys. Rev. A*, 2016, **94**, 022712.
19 P. Bhatt, T. Sairam, A. Kumar, H. Kumar and C. P. Safvan, *Phys. Rev. A*, 2017, **96**, 022710.
20 R. Plašil, S. Rednyk, A. Kovalenko, T. D. Tran, Š. Roučka, P. Dohnal, O. Novotný and J. Glosík, *Astrophys. J.*, 2021, **910**, 155.
21 R. Thissen, O. Witasse, O. Dutuit, C. S. Wedlund, G. Gronoff and J. Lilensten, *Phys. Chem. Chem. Phys.*, 2011, **13**, 18264–18287.
22 O. Dutuit, N. Carrasco, R. Thissen, V. Vuitton, C. Alcaraz, P. Pernot, N. Balucani, P. Casavecchia, A. Canosa, S. Le Picard, J.-C. Loison, Z. Herman, J. Zabka, D. Ascenzi, P. Tosi, P. Franceschi, S. D. Price and P. Lavvas, *Astrophys. J., Suppl. Ser.*, 2013, **204**, 20.
23 C. L. Ricketts, D. Schröder, C. Alcaraz and J. Roithová, *Chem. – Eur. J.*, 2008, **14**, 4779–4783.

Open Access Article. Published on 22 March 2022. Downloaded on 2/21/2026 4:14:56 PM.
This article is licensed under a Creative Commons Attribution 3.0 Unported Licence.

24 E.-L. Zins and D. Schröder, *J. Phys. Chem. A*, 2010, **114**, 5989–5996.
25 J. Roithová and D. Schröder, *Chem. – Eur. J.*, 2007, **13**, 2893–2902.
26 J. Roithová and D. Schröder, *Phys. Chem. Chem. Phys.*, 2007, **9**, 731–738.
27 L. A. Frank, W. R. Paterson, K. L. Ackerson, V. M. Vasyliunas, F. V. Coroniti and S. J. Bolton, *Science*, 1996, **274**, 394–395.
28 H. Gu, J. Cui, D. Niu, L. Dai, J. Huang, X. Wu, Y. Hao and Y. Wei, *Earth Planet. Phys.*, 2020, **4**, 396–402.
29 H. Sabzyan, E. Keshavarz and Z. Noorisafa, *J. Iran. Chem. Soc.*, 2014, **11**, 871–945.
30 S. Falcinelli, F. Pirani, M. Alagia, L. Schio, R. Richter, S. Stranges, N. Balucani and F. Vecchiocattivi, *Atmosphere*, 2016, **7**, 112.
31 S. Falcinelli, M. Rosi, P. Candori, F. Vecchiocattivi, J. M. Farrar, F. Pirani, N. Balucani, M. Alagia, R. Richter and S. Stranges, *Planet. Space Sci.*, 2014, **99**, 149–157.
32 J. Lilensten, C. Simon Wedlund, M. Barthélémy, R. Thissen, D. Ehrenreich, G. Gronoff and O. Witasse, *Icarus*, 2013, **222**, 169–187.
33 M. Alagia, N. Balucani, P. Candori, S. Falcinelli, F. Pirani, R. Richter, M. Rosi, S. Stranges and F. Vecchiocattivi, *Rend. Lincei*, 2013, **24**, 53–65.
34 J. C. Laas and P. Caselli, *Astron. Astrophys.*, 2019, **624**, A108.
35 C. T. Russell and M. G. Kivelson, *Science*, 2000, **287**, 1998–1999.
36 M. Kumar and J. S. Francisco, *Proc. Natl. Acad. Sci. U. S. A.*, 2017, **114**, 864–869.
37 X. Zhang, M. C. Liang, F. Montmessin, J. L. Bertaux, C. Parkinson and Y. L. Yung, *Nat. Geosci.*, 2010, **3**, 834–837.
38 W. W. Kellogg, R. D. Cadle, E. R. Allen, A. L. Lazrus and E. A. Martell, *Science*, 1972, **175**, 587–596.
39 L. A. Komarnisky, R. J. Christopherson and T. K. Basu, *Nutrition*, 2003, **19**, 54–61.
40 J. N. Bull, J. W. L. Lee and C. Vallance, *Phys. Rev. A*, 2017, **96**, 042704.
41 M. Hochlaf, R. Linguerri, M. Cheraki, T. Ayari, R. Ben Said, R. Feifel and G. Chambaud, *J. Phys. Chem. A*, 2021, **125**, 1958–1971.
42 T. Barker, *Astrophys. J.*, 1980, **240**, 99–104.
43 S. Rappaport, E. Chiang, T. Kallman and R. Malina, *Astrophys. J.*, 1994, **431**, 237–246.
44 L. T. Greenberg, P. Dyal and T. R. Geballe, *Astrophys. J., Lett.*, 1977, **213**, L71–L74.
45 D. E. Shemansky and G. R. Smith, *J. Geophys. Res.*, 1981, **86**, 9179–9192.
46 F. Bagenal and J. D. Sullivan, *J. Geophys. Res.: Space Phys.*, 1981, **86**, 8447–8466.
47 F. Herbert, N. M. Schneider, A. R. Hendrix and F. Bagenal, *J. Geophys. Res.: Space Phys.*, 2003, **108**, 1167.
48 S. Kumar, *Icarus*, 1985, **61**, 101–123.
49 J. R. Spencer and N. M. Schneider, *Annu. Rev. Earth Planet. Sci.*, 1996, **24**, 125–190.
50 P. A. Delamere and F. Bagenal, *J. Geophys. Res.*, 2003, **108**, 1276.
51 R. C. Allen, C. P. Paranicas, F. Bagenal, S. K. Vines, D. C. Hamilton, F. Allegrini, G. Clark, P. A. Delamere, T. K. Kim, S. M. Krimigis, D. G. Mitchell, T. H. Smith and R. J. Wilson, *Geophys. Res. Lett.*, 2019, **46**, 11709–11717.
52 G. Clark, B. H. Mauk, C. Paranicas, P. Kollmann and H. T. Smith, *J. Geophys. Res.: Space Phys.*, 2016, **121**, 2264–2273.
53 D. F. Mark, F. M. Stuart and M. de Podesta, *Geochim. Cosmochim. Acta*, 2011, **75**, 7494–7501.
54 S. A. Stern, *Rev. Geophys.*, 1999, **37**, 453–491.
55 A. O. Nier, W. B. Hanson, A. Seiff, M. B. McElroy, N. W. Spencer, R. J. Duckett, T. C. Knight and W. S. Cook, *Science*, 1976, **193**, 786–788.
56 H. B. Niemann, S. K. Atreya, G. R. Carignan, T. M. Donahue, J. A. Haberman, D. N. Harpold, R. E. Hartle, D. M. Hunten, W. T. Kasprzak, P. R. Mahaffy, T. C. Owen, N. W. Spencer and S. H. Way, *Science*, 1996, **272**, 846–849.
57 W. B. Hubbard and M. S. Marley, *Icarus*, 1989, **78**, 102–118.
58 L. Wallace, *Icarus*, 1980, **43**, 231–259.
59 A. G. W. Cameron, *Space Sci. Rev.*, 1973, **15**, 121–146.
60 D. D. Bogard, R. N. Clayton, K. Marti, T. Owen and G. Turner, in *Space Science Reviews*, ed. R. Kallenbach, J. Geiss and W. K. Hartmann, Springer, Dordrecht, 2001, vol. 12, pp. 425–458.
61 H. B. Niemann, S. K. Atreya, J. E. Demick, D. Gautier, J. A. Haberman, D. N. Harpold, W. T. Kasprzak, J. I. Lunine, T. C. Owen and F. Raulin, *J. Geophys. Res.*, 2010, **115**, E12006.
62 O. Badr and S. D. Probert, *Appl. Energy*, 1993, **46**, 1–67.
63 E. W. Schwieterman, T. D. Robinson, V. S. Meadows, A. Misra and S. Domagal-Goldman, *Astrophys. J.*, 2015, **810**, 57.
64 D. Smith, D. Grief and N. G. Adams, *Int. J. Mass Spectrom. Ion Phys.*, 1979, **30**, 271–283.
65 D. Smith, N. G. Adams, E. Alge, H. Villinger and W. Lindinger, *J. Phys. B: At. Mol. Phys.*, 1980, **13**, 2787–2799.
66 G. Dupeyrat, J. B. Marquette, B. R. Rowe and C. Rebrion, *Int. J. Mass Spectrom. Ion Processes*, 1991, **103**, 149–156.
67 G. C. Shields and T. F. Moran, *J. Phys. B: At. Mol. Phys.*, 1983, **16**, 3591–3607.
68 E. Y. Kamber, P. Jonathan, A. G. Brenton and J. H. Beynon, *J. Phys. B: At. Mol. Phys.*, 1987, **20**, 4129–4142.
69 S. M. Harper, W.-P. Hu and S. D. Price, *J. Phys. B: At., Mol. Opt. Phys.*, 2002, **35**, 4409–4423.
70 H. R. Koslowski, H. Lebius, V. Staemmler, R. Fink, K. Wiesemann and B. A. Huber, *J. Phys. B: At., Mol. Opt. Phys.*, 1991, **24**, 5023–5034.
71 E. L. Zins and D. Schröder, *Int. J. Mass Spectrom.*, 2011, **299**, 53–58.
72 J. Roithová, Z. Herman, D. Schröder and H. Schwarz, *Chem. – Eur. J.*, 2006, **12**, 2465–2471.
73 J. Roithová, R. Thissen, J. Žabka, P. Franceschi, O. Dutuit and Z. Herman, *Int. J. Mass Spectrom.*, 2003, **228**, 487–495.
74 N. Tafadar, N. Kaltsoyannis and S. D. Price, *Int. J. Mass Spectrom.*, 1999, **192**, 205–214.
75 P. W. Burnside and S. D. Price, *Int. J. Mass Spectrom.*, 2006, **249–250**, 279–288.
76 W.-P. Hu, S. M. Harper and S. D. Price, *Mol. Phys.*, 2005, **103**, 1809–1819.

 This journal is © the Owner Societies 2022

Open Access Article. Published on 22 March 2022. Downloaded on 2/21/2026 4:14:56 PM. This article is licensed under a Creative Commons Attribution 3.0 Unported Licence.

77 M. Manning, S. D. Price and S. R. Leone, *J. Chem. Phys.*, 1993, **99**, 8695–8704.
78 S. D. Price, M. Manning and S. R. Leone, *Chem. Phys. Lett.*, 1993, **214**, 553–558.
79 D. Ascenzi, P. Tosi, J. Roithová, C. L. Ricketts, D. Schröder, J. F. Lockyear, M. A. Parkes and S. D. Price, *Phys. Chem. Chem. Phys.*, 2008, **10**, 7121–7128.
80 J. F. Lockyear, K. Douglas, S. D. Price, M. Karwowska, K. J. Fijalkowski, W. Grochala, M. Remeš, J. Roithová and D. Schröder, *J. Phys. Chem. Lett.*, 2010, **1**, 358–362.
81 H. Störi, E. Alge, H. Villinger, F. Egger and W. Lindinger, *Int. J. Mass Spectrom. Ion Phys.*, 1979, **30**, 263–270.
82 J. Roithová, J. Žabka, Z. Herman, R. Thissen, D. Schröder and H. Schwarz, *J. Phys. Chem. A*, 2006, **110**, 6447–6453.
83 J. Roithová, J. Žabka, J. Hrušák, R. Thissen and Z. Herman, *J. Phys. Chem. A*, 2003, **107**, 7347–7354.
84 J. Jašik, J. Roithová, J. Žabka, R. Thissen, I. Ipolyi and Z. Herman, *Int. J. Mass Spectrom.*, 2006, **255–256**, 150–163.
85 K. A. Newson and S. D. Price, *Chem. Phys. Lett.*, 1997, **269**, 93–98.
86 Z. Herman, J. Žabka, Z. Dolejšek, M. Fárník and M. Fárník, *Int. J. Mass Spectrom.*, 1999, **192**, 191–203.
87 N. Lambert, N. Kaltsoyannis, S. D. Price, J. Žabka and Z. Herman, *J. Phys. Chem. A*, 2006, **110**, 2898–2905.
88 N. Tafadar and S. D. Price, *Int. J. Mass Spectrom.*, 2003, **223–224**, 547–560.
89 J. F. Lockyear, C. L. Ricketts, M. A. Parkes and S. D. Price, *Chem. Sci.*, 2011, **2**, 150–156.
90 S. Armenta Butt and S. D. Price, *Phys. Chem. Chem. Phys.*, 2021, **23**, 11287–11299.
91 H. M. Holzscheiter and D. A. Church, *J. Chem. Phys.*, 1981, **74**, 2313–2318.
92 P. Tosi, R. Correale, W. Lu, S. Falcinelli and D. Bassi, *Phys. Rev. Lett.*, 1999, **82**, 450–452.
93 A. Ehbrecht, N. Mustafa, C. Ottinger and Z. Herman, *J. Chem. Phys.*, 1996, **105**, 9833–9846.
94 J. H. Agee, J. B. Wilcox, L. E. Abbey and T. F. Moran, *Chem. Phys.*, 1981, **61**, 171–179.
95 S. M. Harper, S. W.-P. Hu and S. D. Price, *J. Chem. Phys.*, 2004, **120**, 7245–7248.
96 B. K. Chatterjee and R. Johnsen, *J. Chem. Phys.*, 1989, **91**, 1378–1379.
97 G. Niedner-Schatteburg, T. Schindler, C. Berg, D. Wössner and V. E. Bondybey, *J. Chem. Phys.*, 1993, **99**, 9664–9669.
98 W.-P. Hu, S. M. Harper and S. D. Price, *Meas. Sci. Technol.*, 2002, **13**, 1512–1522.
99 S. D. Price, *Int. J. Mass Spectrom.*, 2007, **260**, 1–19.
100 K. M. Douglas and S. D. Price, *Int. J. Mass Spectrom.*, 2011, **303**, 147–153.
101 K. Yamasaki and S. R. Leone, *J. Chem. Phys.*, 1989, **90**, 964–976.
102 J. F. Lockyear, M. A. Parkes and S. D. Price, *J. Phys. B: At., Mol. Opt. Phys.*, 2009, **42**, 145201.
103 *NIST Atomic Spectra Database (version 5.6.1)*, ed. A. Kramida, Y. Ralchenko, J. Reader and NIST ASD Team, National Institute of Standards and Technology, Gaithersburg, MD, 2020.
104 W. C. Martin, R. Zalubas and A. Musgrove, *J. Phys. Chem. Ref. Data*, 1990, **19**, 821–880.
105 N. Imadouchene, H. Aouchiche and C. Champion, *J. Electron Spectrosc. Relat. Phenom.*, 2016, **210**, 36–48.
106 M. V. V. S. Rao and S. K. Srivastava, *J. Geophys. Res.*, 1993, **98**, 13137–13145.
107 T. Nakamura, N. Kobayashi and Y. Kaneko, *J. Phys. Soc. Jpn.*, 1985, **54**, 2774–2775.
108 S. J. Smith, J. B. Greenwood, A. Chutjian and S. S. Tayal, *Astrophys. J.*, 2000, **541**, 501–505.
109 H. W. Moos, S. T. Durrance, T. E. Skinner, P. D. Feldman, J.-L. Bertaux and M. C. Festou, *Astrophys. J.*, 1983, **275**, L19–L23.
110 P. L. Smith, C. E. Magnusson and P. O. Zetterberg, *Astrophys. J.*, 1984, **277**, L79.
111 L. I. Podobedova, D. E. Kelleher and W. L. Wiese, *J. Phys. Chem. Ref. Data*, 2009, **38**, 171–439.
112 Z. Herman, *Int. Rev. Phys. Chem.*, 1996, **15**, 299–324.
113 S. A. Rogers, S. D. Price and S. R. Leone, *J. Chem. Phys.*, 1993, **98**, 280–289.
114 S. D. Price, *J. Chem. Soc., Faraday Trans.*, 1997, **93**, 2451–2460.
115 M. A. Parkes, J. F. Lockyear and S. D. Price, *Int. J. Mass Spectrom.*, 2009, **280**, 85–92.
116 G. Dujardin, M. J. Besnard, L. Hellner and Y. Malinovitch, *Phys. Rev. A: At., Mol., Opt. Phys.*, 1987, **35**, 5012–5019.
117 B. Godard, E. Falgarone, M. Gerin, D. C. Lis, M. De Luca, J. H. Black, J. R. Goicoechea, J. Cernicharo, D. A. Neufeld, K. M. Menten and M. Emprechtinger, *Astron. Astrophys.*, 2012, **540**, A87.
118 F. Lique, A. Zanchet, N. Bulut, J. R. Goicoechea and O. Roncero, *Astron. Astrophys.*, 2020, **638**, A72.
119 D. O. Kashinski, D. Talbi, A. P. Hickman, O. E. Di Nallo, F. Colboc, K. Chakrabarti, I. F. Schneider and J. Z. Mezei, *J. Chem. Phys.*, 2017, **146**, 204109.
120 P. J. Dagdigian, *J. Chem. Phys.*, 2019, **150**, 84308.
121 P. Bolognesi, L. Avaldi, M. A. MacDonald, C. M. A. Lopes, G. Dawber, C. E. Brion, Y. Zheng and G. C. King, *Chem. Phys. Lett.*, 1999, **309**, 171–176.
122 L. Åsbrink, *Chem. Phys. Lett.*, 1970, **7**, 549–552.
123 F. Merkt and T. P. Softley, *J. Chem. Phys.*, 1992, **96**, 4149–4156.
124 K. M. Weitzel, J. Mähnert and M. Penno, *Chem. Phys. Lett.*, 1994, **224**, 371–380.
125 R. B. Cordaro, K. C. Hsieh and L. C. McIntyre Jr, *J. Phys. B: At. Mol. Phys.*, 1986, **19**, 1863–1872.
126 R. Stockbauer, *J. Chem. Phys.*, 1979, **70**, 2108–2114.
127 J. L. Gardner and J. A. R. Samson, *J. Electron Spectrosc. Relat. Phenom.*, 1976, **8**, 123–127.
128 T. E. Sharp, *At. Data Nucl. Data Tables*, 1970, **2**, 119–169.
129 M. Beyer and F. Merkt, *J. Mol. Spectrosc.*, 2016, **330**, 147–157.
130 M. Beyer and F. Merkt, *Phys. Rev. Lett.*, 2016, **116**, 093001.
131 M. A. Parkes, J. F. Lockyear, S. D. Price, D. Schröder, J. Roithová and Z. Herman, *Phys. Chem. Chem. Phys.*, 2010, **12**, 6233–6243.
132 C. L. Ricketts, D. Schröder, J. Roithová, H. Schwarz, R. Thissen, O. Dutuit, J. Žabka, Z. Herman and S. D. Price, *Phys. Chem. Chem. Phys.*, 2008, **10**, 5135–5143.

Open Access Article. Published on 22 March 2022. Downloaded on 2/21/2026 4:14:56 PM.
This article is licensed under a Creative Commons Attribution 3.0 Unported Licence.

133 S. Armenta Butt and S. D. Price, *Phys. Chem. Chem. Phys.*, 2020, **22**, 8391–8400.
134 M. A. Parkes, J. F. Lockyear, D. Schröder, J. Roithová and S. D. Price, *Phys. Chem. Chem. Phys.*, 2011, **13**, 18386–18392.
135 S. Strathdee and R. Browning, *J. Phys. B: At. Mol. Phys.*, 1979, **12**, 1789–1804.
136 K. Köllmann, *Int. J. Mass Spectrom. Ion Phys.*, 1975, **17**, 261–285.
137 K. Ito, R. I. Hall and M. Ukai, *J. Chem. Phys.*, 1996, **104**, 8449–8457.
138 C. Bottcher, *J. Phys. B: At. Mol. Phys.*, 1974, **7**, L352.
139 C. J. Latimer, J. Geddes, M. A. MacDonald, N. Kouchi and K. F. Dunn, *J. Phys. B: At., Mol. Opt. Phys.*, 1996, **29**, 6113–6121.
140 In *CRC Handbook of Chemistry and Physics*, ed. J. R. Rumble, CRC Press/Taylor & Francis, Boca Raton, FL, 100th edn, 2020.
141 A. J. Yencha, K. Ellis and G. C. King, *J. Electron Spectrosc. Relat. Phenom.*, 2014, **195**, 160–173.
142 P. Baltzer, M. Larsson, L. Karlsson, B. Wannberg and M. Carlsson Göthe, *Phys. Rev. A: At., Mol., Opt. Phys.*, 1992, **46**, 5545–5553.
143 H. R. Hrodmarsson, R. Thissen, D. Dowek, G. A. Garcia, L. Nahon and T. R. Govers, *Front. Chem.*, 2019, **7**, 222.
144 E. M. Bahati, J. J. Jureta, D. S. Belic, H. Cherkani-Hassani, M. O. Abdellahi and P. Defrance, *J. Phys. B: At., Mol. Opt. Phys.*, 2001, **34**, 2963–2973.
145 X. Tang, Y. Hou, C. Y. Ng and B. Ruscic, *J. Chem. Phys.*, 2005, **123**, 074330.
146 L. Åsbrink and C. Fridh, *Phys. Scr.*, 1974, **9**, 338–340.
147 P. Rivière-Marichalar, A. Fuente, J. R. Goicoechea, J. Pety, R. Le Gal, P. Gratier, V. Guzmán, E. Roueff, J. C. Loison, V. Wakelam and M. Gerin, *Astron. Astrophys.*, 2019, **628**, A16.
148 T. Trabelsi, S. Ben Yaghlane, M. M. Al Mogren, J. S. Francisco and M. Hochlaf, *J. Chem. Phys.*, 2016, **145**, 084307.
149 M. Canaves, A. A. De Almeida, D. C. Boice and G. C. Sanzovo, *Earth, Moon, Planets*, 2002, **90**, 335–347.
150 J. Cernicharo, B. Lefloch, M. Agúndez, S. Bailleux, L. Margulès, E. Roueff, R. Bachiller, N. Marcelino, B. Tercero, C. Vastel and E. Caux, *Astrophys. J., Lett.*, 2018, **853**, L22.
151 S. Ben Yaghlane and M. Hochlaf, *J. Phys. B: At., Mol. Opt. Phys.*, 2009, **42**, 015101.
152 J. Czernek and O. Živný, *Chem. Phys.*, 2004, **303**, 137–142.
153 J. M. Dyke, A. Morris and I. R. Trickle, *J. Chem. Soc., Faraday Trans. 2*, 1977, **73**, 147–151.
154 P. A. G. O'Hare, *J. Chem. Phys.*, 1970, **52**, 2992–2996.
155 A. Karpfen, P. Schuster, J. Petkov and H. Lischka, *J. Chem. Phys.*, 1978, **68**, 3884–3890.
156 K. A. Peterson and R. C. Woods, *J. Chem. Phys.*, 1988, **89**, 4929–4944.
157 D. Zhou, D. Shi, Z. Zhu and J. Sun, *J. Quant. Spectrosc. Radiat. Transfer*, 2019, **224**, 1–8.